A Numerical Model Study of the Coastal Ocean Flow Due to the Turbulence Parameterization

KWANG WOO YOU

Department of Oceanography, Scoul National University, Seoul 151-742, Korea

亂流의 媒介變數化에 따른 沿岸流의 수치모델 연구

柳 光 雨

서울대학교 자연과학대학 해양학과

A three-dimensional time-dependent coastal ocean model experiment of two different turbulence parameterizations is conducted. One of the turbulence parameterization is the constant eddy-mixing formulaton, C1, and the other a stratification dependent eddy-mixing formulation, C2.

The flow in C2 is strongly baroclinic, and limits vertical mixing of fresh and saline waters. The outflow discharged from an estuary is highly inertial and form a strong front of plume in C2 than that in C1. Because of the stronger ouflow in C2, supercritical flow state, for which the near-surface outflow velocity exceeds the baroclinic phase speed, can exist off the mouth of the estuary. The adjustment process of flow in the less saline waters are quite different for C1 and C2, which is dictated by the strongly baroclinic nature of the flow in C2.

두 가지의 서로 다른 亂流 변수화를 삼차원적이고 시간의존적인 연안해역의 모델실험으로 수행하였다. 난류 변수화 중의 하나는 일정한 渦動混合化 한 것, C1이고 다른 하나는 層化 의존적인 와동혼합화, C2이다.

C2를 이용한 유체흐름은 강한 傾壓的 흐름이며 담수와 염수의 수직적인 혼합을 제한하고 있다. 하구언으로부터 방출되는 유출류는 C2의 경우가 C1의 경우보다 훨씬 더 慣性的이며 강한 플륨(plume) 前線을 형성한다. C2에서는 강한 유출류로 인하여 超臨界的인 유체흐름의 상태, 즉 표층류의 유출속도가 경압적 위상속도를 능가하는 상황이 하구언의 외해쪽에 존재할 수 있다. 담수영역에서의 유체의 조율과정은 C1의 경우와 C2의 경우가 상당이 다른 바, C2에서의 유체의 흐름은 강한 경압적인 특성을 보여준다.

INTRODUCTION

How much the turbulence can be improtant to models of dynnamics of estuary plumes and fronts? First of all, the turbulence is expected to be important in the dynamics of estuary plumes and coastal fronts in view of the mixing of fresh and brackish waters. The inclusion of turbulence mixing coefficients which depend on stratification can produce dynamics with entrainment processes caused by differential turbulence intensity in the water column. As a step in understanding how mixing determines variabilities of the flow, the numerical solutions which are obtained from the hypothetical three-dimensional model with two different turbulence parameterizations are examined. They are the constant eddy-mixing formulation, C1, and a stratification dependent formulation, C2.

The plume turns to the right from the viewpoint of an observer at the estuary mouth looking seaward due to the earth rotation when the width of the estuary is larger than about 10 km in the
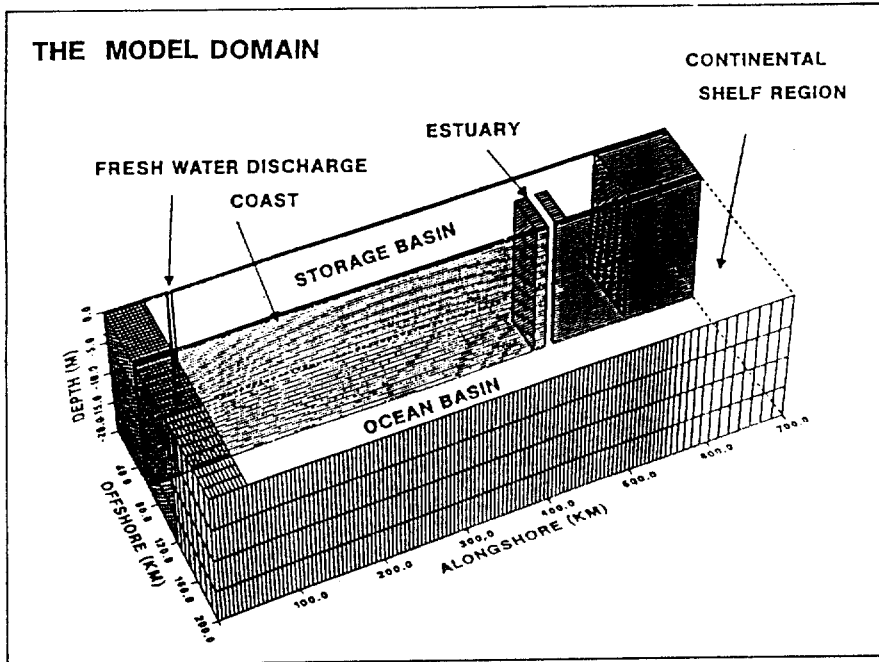
Fig. 1. The three-dimensional model domain. For clarity, the vertical grid and finest grids in the horizontal are plotted at every other grid.

northern hemishere. A coastal front of width of approximately the Rossby radius of deformation, RO. is formed along the shoreline when less-saline water disembogues into an adjacent sea. This complex non-linear problem was first studied by Chao and Boicourt (1986), and Chao (1987, 1988 a. b) using Bryan/Cox (1984) three-dimensional, primitive model with simple turbulence parameterization; constant vertical diffusivity/viscosity for stable stratification, and infinite mixing when unstable. The Chao and Boicourt's model reproduced the expected anticyclonic plume as less-saline water flows out of the estuary's mouth. In the near field, oppositely directed two layer flow develops along coast, while the far-field solution is uni-directional. After initial transient of estuarine water lasting about 5 to 10 days, an anticyclonic plume is formed near the mouth. The plume is quasi-steady in that no major time-dependent events occur thereafter, except a few small-scale sheddings of eddies at the fringe of the plume.

The time-evolution of three-dimensional discharged plume and its coastal front on a model con-

tinental shelf is calculated based on the Mellor and Yamada's (1982) turbulence kinetic energy closure scheme. In the present model, the continental shelf is opened up with a free river boundary which is closed in the Chao and Boicourt's model. An energetic intrusive bore are dumped in the open ocean boundaries and allowed to pass freely. Many of the tested solutions with radiation conditions at the river head were numerically unstable after 100 days or so. This is related to the sensitive up-stream dependence of the coastal front reported by Stern et al. (1982). To avoid the sensible effects on the parameters in the radiation condition, the present model includes a storage basin into which fresh water is pumped, and that connects to the continental shelf through an estuary. Only then can we perform long-term integration of subtidal variability with periods of O(days to months), and at the same time incorporate mixing processes due to winds and tides also.

MODEL FORMULATON

The model domain, shown in Fig. 1 consists

of a continental shelf of dimensions 700 km along-shore (north-south direction) and 140 km cross-shore (east-west direction). The continental shelf connects to a storage basin of width of 60 km and length 600 km through an elongated estuary of length of 39 km and width 15 km. There is an opening 15 km wide near the southwestern corner of the storage basin, across which fresh water is pumped into the basin at a rate of 1000 $m^3 s^{-1}$. The model grid size in the x-direction (cross-shore direction) is 3 km in the region from western boundary in the storage basin to about 50 km offshore on the mid-shelf, and expands linearly to 10 km on the outer-shelf. In the y-direction (along-shore direction), the grid sizes are 3 km in the storage basin, the estuary and over most of shelf, except in the northern-most 140 km of the estuary, where the grid expands linearly to 13 km. The grid sizes are almost constant over most of the model domain in order to retain second order accuracy. There are ten levels over the vertical water column of constant depth 20 m, so that each water layer is 2 m.

The σ coordinate system is applied in the z-direction. The relative positions of the variables are assigned on the staggered computational C grid system. The model solves the finite-difference analog of the following set of equations with hydrostatic assumption and Boussinesq approximation.

$$\Delta \cdot u + w_z = 0 \tag{1}$$

$$\begin{aligned} u_t + u \cdot \Delta u + w u_z + fkxu \\ = -\Delta p/\rho_0 + (K_M \ u_z)_z + F_M \end{aligned} \tag{2}$$

$$\rho g = -p_z \tag{3}$$

$$e_t + u \cdot \Delta e + w e_z = (K_H \ e_z)_z + F_H \tag{4}$$

$$\rho = (T, \ S) \tag{5}$$

where x, y and z form a right-handed Cartesian coordinate system with positive x eastward, positive y northward, positive z upward, and k is unit vector, and t is the time. Here, Δ is the horizontal gradient operator, $u = (u,v)$ is the horizontal velocity vector, w is the vertical component of velocity, ρ_0 is a reference density, p and ρ are deviation pressure and density, respectively; e denote either the temperature T or the salinity S, which are related to through the equation of state (equation

(5)), f is the Corilois parameter. For the present model, T is set constant at 10°C. The motions induced by subgrid scale processes are parameterized in terms of horizontal mixing processes. The FM term in the Reynolds momentum equation (equation (2)) is analogous diffusion terms which are imbeded the horizontal diffusivity A_m. For the present model, the horizontal viscosity/diffusivity coefficient, A_m, is 10 $m^2 s^{-1}$ over most of the model domain except open boundaries, where it is increased for use in conjunction with the radiation conditions there. Vertical turbulent mixing is modeled through the use of the eddy viscosities and diffusivities, K_M and K_H, respectively, according to the level 2.5 turbulence kinetic energy closure of Mellor and Yamada (1982). They are proportional to the turbulence kinetic energy and turbulence macro scale, and are solved by means of advective-diffusive transport equation (Blumberg and Mellor, 1983). Vertical mixing thus depends on the density and veolocity fields, inhibitated by stratification, and intensified by vertical shears and destratification. Details of these and of the numerical method, which includes leapfrog time differencing with split external and internal modes, horizontal spatial differencing which conserve linear and quadratic quatities, vertical sigma coordinates in implicit form with tridiagonal solver and other modelling techniques etc., can be found in Oey et al (1985), You et al (1991) and You and Oh (1993), and are not repeated here.

Time-integration is split into a two-dimensional, external mode with a short time-step which is controlled by the free-surface gravity wave speed, and a three-dimensional, internal mode with a long time-step calculated using the internal wave speed. For the present simulation, the time step for the internal three-dimensional calculation is 800 seconds, and is 80 seconds for the depth-averaged external two-dimensional calculation of transport and surface elevation.

BOUNDARY CONDITIONS

The open ocean boundary specifications are the most difficult, yet they are essential for a long-time

and time-dependent simulation. They can contaminate interior solutions if mishandled. For example, if the open ocean boundary is a wall or acts like a wall, the intrusive bore propagates southward along the coast then the nose either turns seaward along the southern, cross-shelf boundary. Therefore, the flow must be allowed to continue southward by some appropriate boundary conditions. Otherwise, the nose will circle around open ocean boundaries and eventually return to the solution region of interest at the estuary mouth. In the present model calculation, the dissipative layers coupled with Oranski's (1976) radiation conditions are used. The horizontal diffusivity/viscosity, A_m, is variable such that along the northern and eastern open boundaries where x and y are enlarged, A_m is larger than the basic value of $10\ m^2s^{-1}$ used in the interior to reduce the sensitivity of the up-stream effects on the interior solutions (Stern et al., 1982).

$$A_m = 10\ exp\{d_1[(dx^2+dy^2)^{1/2}-d_2]\} \qquad (6)$$

where $d_2=(dx^2+dy^2)^{1/2}$ is grid distance corresponding to the interior grid sizes $dx=dy=3$ km. The d_1 is a constant value to get $A_m=100\ m^2s^{-1}$ along the northern open boundary where $dy=1.3\times10^4$ m. The usual method in which solution near an open boundary is relaxed back to some climatology, i.e., the use of sponge layers, is not sufficient for the present energetic intrusive bores simulation. There are dissipative layers near open boundaries where waves are partially absorbed so that the perturbation exit boundary as smoothly as possible. The proper horizontal cross and along boundary diffusivity/viscosity coefficients permit sufficient damping and prevent up-stream reflections and offshore spreadings near the southern boundary. These enhanced diffusion near open boundaries are coupled with radiation.

At the ocean floor, salt flux is zero while momentum flux is balanced by quadratic bottom stress computed using the velocity nearest to the bottom. Salt and momentum fluxes at the free surface are set to zero. The inflow velocity profiles from the southwestern opening is x-directed and is linear with water depth. The calculation starts

with fresh water ($S=0‰$) in the storage basin, and salt water ($S=35‰$) in the estuary and the continental shelf.

For the external mode, elevations along the eastern, southern and northern boundaries, and the normal component of the depth-averaged velocities, a modified Oranski's (1976) radiation condition by adding friction and forcing is used;

$$U_t+CU_n=(U_F-U)/T_i \qquad (7)$$

where U denotes a variable, n is the outward normal, $C=(gH)^{1/2}$, U_F is the forcing and T_i is a time scale taken to be 3 hours. Here, the elevation along the southern and northern boundaries are required only for the calculation of the non-linear advective terms on the staggered grid in the y-momentum equations. Along the eastern boundary, the x-momentum equation is linearized and chosen to specify elevation, rather than the x-component velocity. Along all open boundaries, free-slip conditions are used for the tangential velocity.

The radiation condition is used for both the normal and tangential three-dimensional velocities, in which the C is changed to the internal wave phase speed, C_i, based on the top-to-bottom density difference at one grid point inside the boundary and half depth of the water column, and T_i is proportionately increased by a factor $(C/C_i)^{1/2}$.

For salinity,

$$S_t+n\cdot u_n S_n=0$$

where for inflow, S_n is approximated by (S_F-S) /dn, where dn is the grid size normal to boundary, and for outflow one-sided difference is used. The salinity forcing S_F can in general be a fuction of distance along the bounday, as well as of water depth, z.

$$S_F(z)=35.0-(z+H)/2H \qquad (9)$$

Open boundary values of other model variables like turbulence length scale and kinetic energy are less crucial to the solution and are therefore extrapolated from interior values by assuming zero normal gradients. The open boundary conditions used here allow free development of the baroclinic structure of the model ocean. For realistic simula-
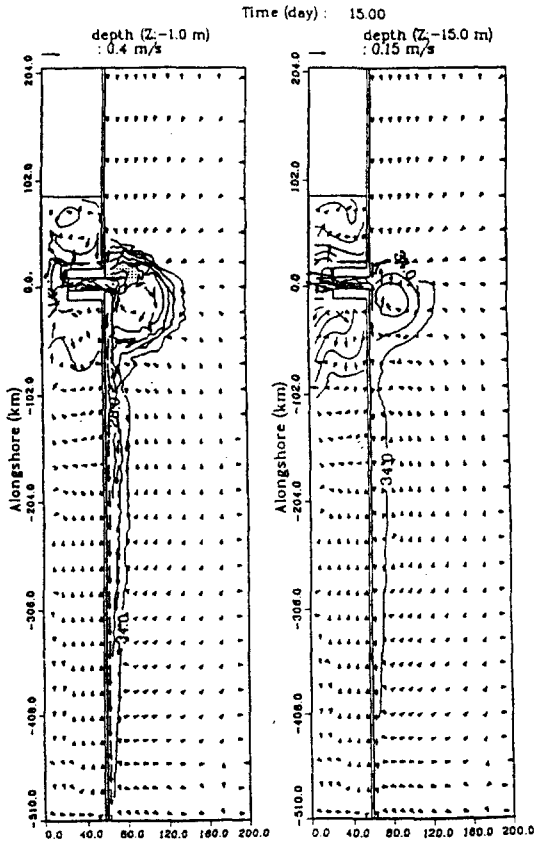
Fig. 2a. The velocity vectors and salinity at z= −1 m (left pannel) and −15 m (right pannel) at time t= 15 days for the model calculation with constant eddy-mixing coefficients. The contour interval is 3‰, and vectors are plotted at every other two grid points. Regions where 20‰<S<23‰ in the surface layers are stippled.

Fig. 2b. As in Fig. 2a except at time t=20 days.

tions when tides and cross-bounday transports are specified, one can expects that after an adjustment period there will be balances in both volume and salt fluxes, as they must be in a real ocean.

MODEL RESULTS

The Constant Eddy-Mixing Formulation (C1) Experiment

When the eddy-mixing coefficient depends on stratification, more complex dynamics occur as a result of differential turbulence intensities in the water column. However, the more fundamental
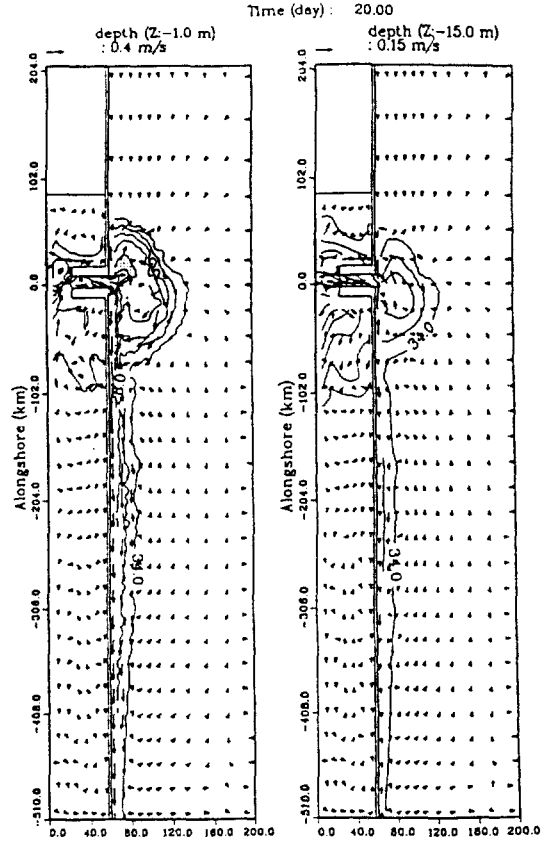
phenomena such as frontal meander and its growth can be seen also in a model with a constant eddy-mixing coefficient.

The velocity vectors and salinity contours, at z= −1.0 m (left pannel) and −15.0 m (right pannel), and at t= 15, 20, 32, 50 and 80 days are shown in Fig. 2a through Fig. 2e for the model calculation with a constant eddy mixing coefficient. The salinity contour interval is 3.0‰, and velocity vectors are plotted at other two grid points for clarity. There are several important dynamics. First, the open boundary conditions used in the present model give little spurious solution near boundaries. Along the southern boundary, for example, a non-radiating condition would act like a wall along which the nose of the intrusive bore would propagate, and this would have shown up as excessive offshore spreadings of less-saline waters. Instead, salinity contours at the 15th and 20th
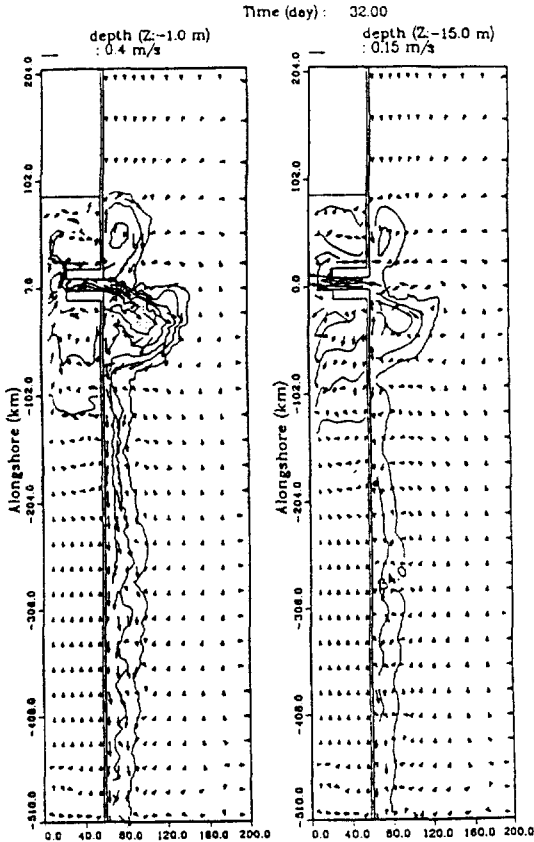
Time (day) :   32.00

depth (Z₋-1.0 m)   depth (Z₋-15.0 m)
: 0.4 m/s   : 0.15 m/s

Time (day) :   50.00

depth (Z₋-1.0 m)   depth (Z₋-15.0 m)
: 0.4 m/s   : 0.15 m/s

Fig. 2c. As in Fig. 2a except at time t=32 days.

Fig. 2d. As in Fig. 2a except at time t=50 days.

day (Figs. 2a and 2b), when the bore begins to cross the southern boundary, show smooth transition near the boundary. Fig. 3 shows an along-boundary/time contour plot of the near-surface salinity ($z = -1.0$ m) at 1.5 km away from the boundary. The along-boundary distance is measured on the shelf from just south of the estuary mouth, southward to the southern cross-shore boundary $(0 \sim 510$ km), then seaward along the cross-shore bounday $(510 \sim 700$ km). Fig. 3 where hatched areas denote $26\%_0 < S < 28\%_0$ shows along-coast bore intrusion for the first 5 to 10 days. At the southern boundary, most of the flow energy passes: some waves seem to be reflected back, but very little intrusion occurs along the boundary. Instead. a slow diffusive process is obvious from the nearly 90 degrees anti-clockwise turn of the contours for along-boundary distance greater than about 520· km. For time greater than about 60
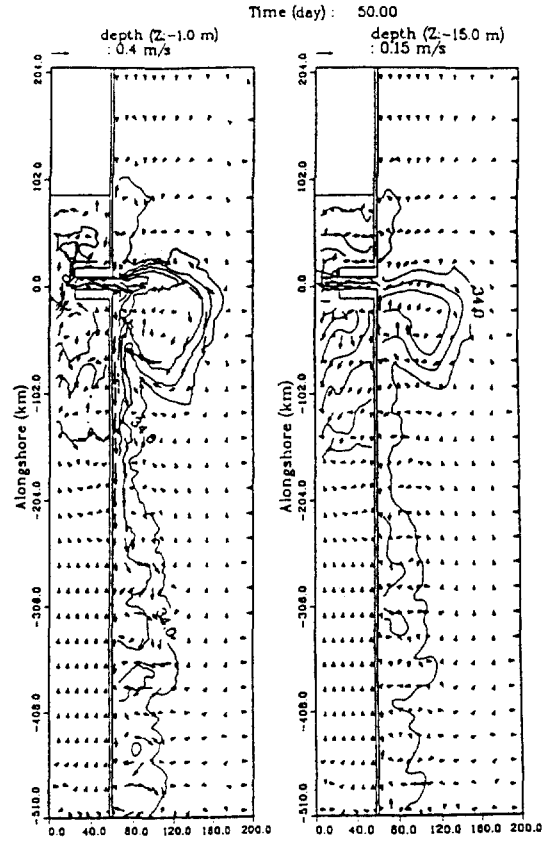
days, offshore spreadings of the coastal front begins to expand toward offshore.

Secondly, Figs. 2 show anticyclonic turn of the plume at the mouth of the estuary, as in Chao and Boicourt (1986). A minor difference here is the appearene of a small, along-shore northward spread of the plume along the northern side of the estuary mouth. This is in part caused by eddy-shedding, and in part by pressure set-down of the free-surface at north (and south) of the plume. Eddy-shedding is also found by Chao and Boicourt, but surface set-down is absent from Chao and Boicourt's rigid-lid model. Near the coast, bottom northward flow is restricted within about 30 km south of the estuary mouth. and that the far-field is uni-directional.

Finally, Figs. 2 show along-shore frontal meanders which develop for t>20 days (Figs. 2b through 2e). These meanders have wavelengths of
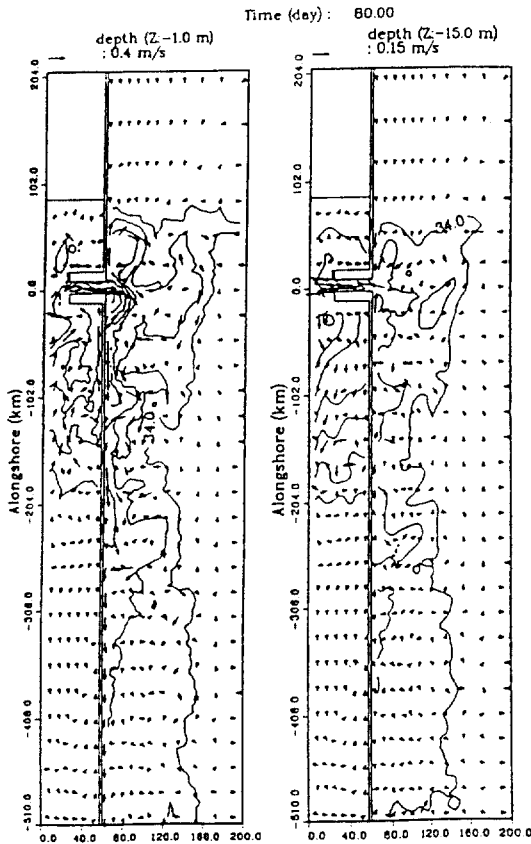
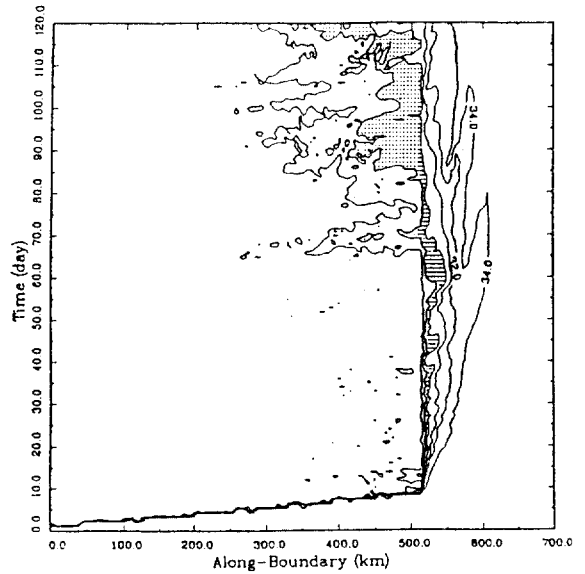Fig. 2e. As in Fig. 2a except at time t=80 days.

Fig. 3. Along-boundary/time contour plot of the near-surface salinity at 1.5 km away from the boundary. The along-boundary distance is measured from just south of the estuary mouth, southward of the southern cross-shore boundary, then seaward along the cross-shore boundary.

km).

Stability Analysis

about 30 km, or approximately $2R_0$. Here

$$R_0=1/f\{0.5\times hg\ (d\rho/\rho_o)\}^{1/2} \qquad (10)$$

where $h=H/2$, is the baroclinic Rossby radius based on $d\rho/\rho_o=2\times10^{-2}$. Wave amplitude increases down-coast. The waves for $32>t>20$ days are similar to those found by Garvine (1987), which shows a doubling of amplitude every 10 R_0. While down-coast wave amplification can be seen from Figs. 2 (in particular, Fig. 2c for -300 km$<y<-100$ km), the doubling cannot be ascertained, probably because waves are developing down-coast, but not stationary as in Garvine's. The short wavelength values suggest instability of barotropic origin. At later times, $t=50$ and 80 days (Figs. 2d and 2e), longer waves indicative of baroclinic instability appear. At these time, cross-shelf jet with velocities of O (0.1 ms^{-1}) are present (Fig. 2d, $y=-260$ km and -350 km; Fig. 2e, $y=-200$ km and -280

The stability analysis is a convinient methods in investigating the pass of energy transfer through a certain interesting route by separating the model solution, denoted by subscripts T for total, into a mean, denoted by subscripts M, plus perturbation. Thus

$$u_T=u_M+U \qquad (11)$$
$$S_T=S_M+s \qquad (12)$$

The mean is obtained from a temporal and along-coast average of the respective field variables. The path of the stability analysis is for shelf region southward from the southern-most grid off the estuary mouth to southern open boundary, and includes part of the discharged plume.

The total pertubation energy (TEP) is a sum of perturbation potetential energy (PEP) and perturbation kinetic energy (KEP).
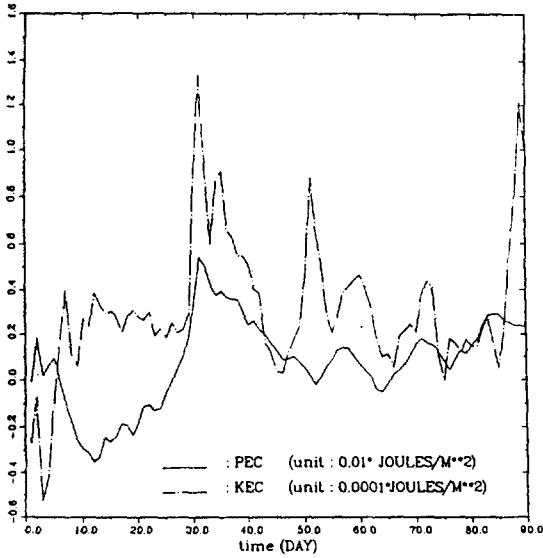
$$PEP=0.5\times(\rho/\rho_n)^2(g^2/N^2) \qquad (13)$$

Fig. 4a. Plots of PEC and KEC as function of time from 0 to 90 days. Note that the KEC has been magnified for clarity.

Fig. 4b. Plots of PEP and KEP as function of time from 0 to 90 days. Note that the KEP has been magnified for clarity.

$$KEP = 0.5 \times (u^2 + v^2) \qquad (14)$$

where, $g = 9.8$ ms^{-2}, the acceleration due to gravity. $N^2 = (-g/\rho_o)(d\rho_o/dz)$, is the squared Brunt-Vaisala frequency and $\rho_o(z)$ is a background density obtained by averaging $\rho_M(x, z)$ over the cross-shelf direction. The rate of change of TEP integrated over the region being analyzed (Oranski and Cox, 1973) is

$$\iiint (TEP)_t \, dxdydz = \iint (KEC + PEC) \, dxdz \qquad (15)$$

where KEC is the kinetic energy (barotropic) conversion term and PEC the potential energy (baroclinic) conversion term, given by

$$KEC = \int (uvv_{Mx} - uwv_{Mz}) \, dy \qquad (16)$$

$$PEC = -(g^2/\rho_o^2 N^2) \int (\rho u \rho_{Mx}) \, dy \qquad (17)$$

Fig. 4 shows plots of PEC, KEC, PEP and KEP as functions of time from 0 to 90 days. Note that the KEC and KEP in these plots have been magnified for clarity. The first seven days are a period of positive potential energy conversion (PEC), caused by intrusion of fresh water onto the continental shelf in the surface layer. The growth of perturbation, both d(TEP)/dt and PEC>0, is by the large vertical shears that are produced, near the estuary
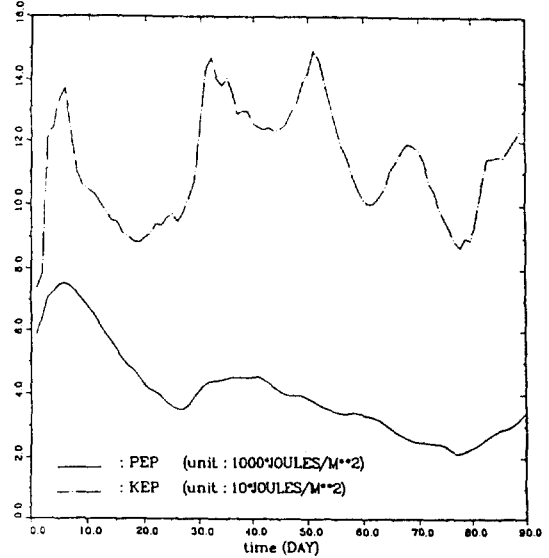
mouth, as well as at the nose of the intrusive bore along the coast. From day 7 through about 30, PEC becomes negative, which means that the conversion path of potential energy is from perturbation to the mean. This is because of a bouyancy source at the estuary mouth, and the mean coastal front strengthens. At the same time, large horizontal shears begin to develop cross the front, and KEC becomes positive. However, PEC is dominant and d(TEP)/dt is actually negative during this period. The barotropic conversion process due to the vertical shears in equation (16) is generally smaller than that due to the cross-frontal shears. Thus one may conclude that from day 7 through 30, the vertical shears begin to develop along the entire frontal zone, and the instability becomes a mixed baroclinic/barotropic type (both PEC and KEC are positive). Contour plots at day 32, 50 and 80 (Figs. 2c, 2d and 2e) show development of long waves (wavelength=$2\pi R_o$) characteristics of baroclinic instability process, in addition to shorter wave (wavelength=$2R_o$) of barotopic instability. However, by these times, viscous dissipation becomes significant, and TEP in Fig. 4 shows a decreasing trend with time.
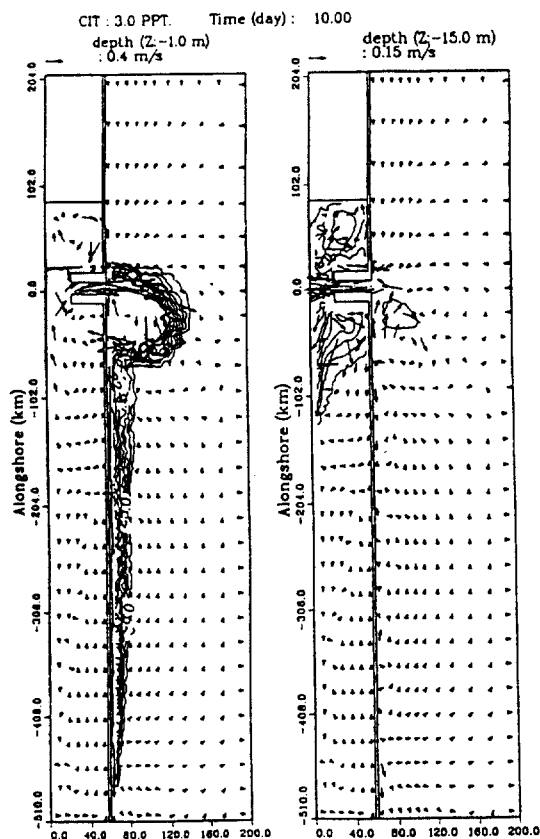
Coastal front resulting from a sudden release

Fig. 5a. The velocity vectors and salinity contours, at z=−1 m (left pannel) and −15 m (right pannel) at time t=10 days for the model calculation based on the turbulence energy closure scheme.

Fig. 5b. As in Fig. 5a except at time t=20 days.

of fresh water over the continental shelf evolves in three phase. The first is a short (about 5 days) intrusive phase when vertical shears are large. There is active exchange of water mass across the fresh/salt water interface and the instability is predominantly baroclinic. The second is a developing phase (about 30 days) during which the coastal front is strengthened by buoyancy supply from the estuary, while the resulting cross-shore shears are intensive enough to trigger barotropic instability with appearance of small amplitude, short wavelength frontal waves. The third is a matured phase during which there is an approximate balance between the buoyancy input from estuary and that lost across the open ocean boundaries. Here, vertical as well as cross-frontal shears are fully establi-
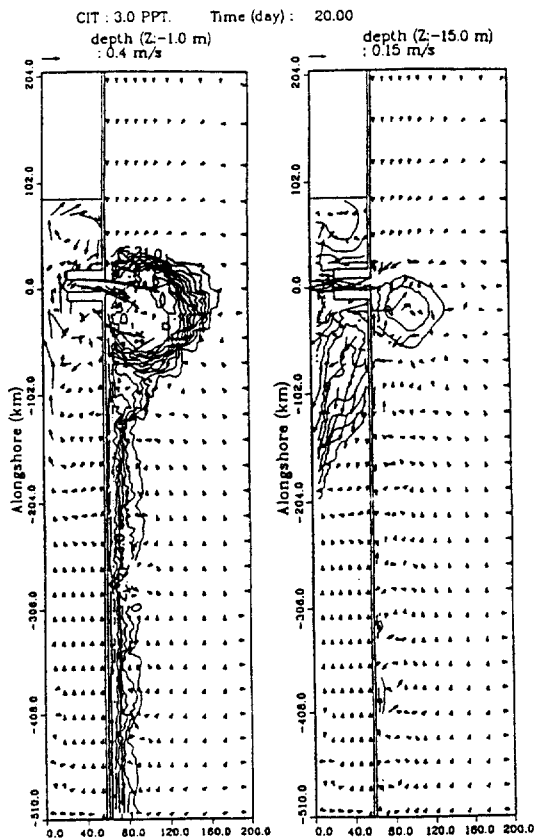
shed and a mixed baroclinic/barotropic type of instability occur, with appearances of both short and long frontal waves. The baroclinic instability appears dominant and result in large amplitude meanders with significant cross-shore flows.

The Turbulence Closure Formulation (C2) Experiment

Figs. 5 show the velocity vectors and salinity contours, at z=−1.0 m (left pannel) and −15.0 m (right pannel), and at t=10, 20, 31, 55, 56, 70, 72 and 73 days for the model calcualtion based on the turbulence energy closure scheme (Mellor and Yamada, 1982). The outer-most contour on the model continental shelf denotes the 34‰ and the contour interval is 3.0‰. For t>55 days, regions where the near-surface salinity is greater than 7.0‰ are cross-hatched.
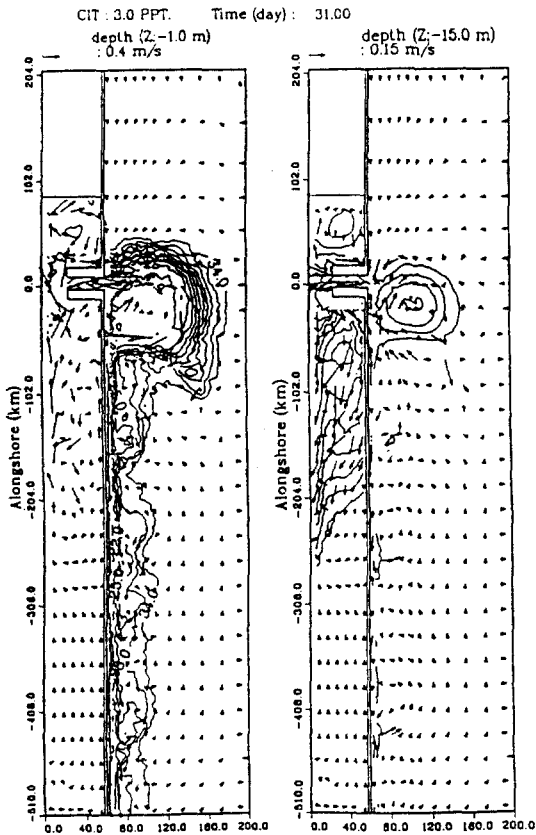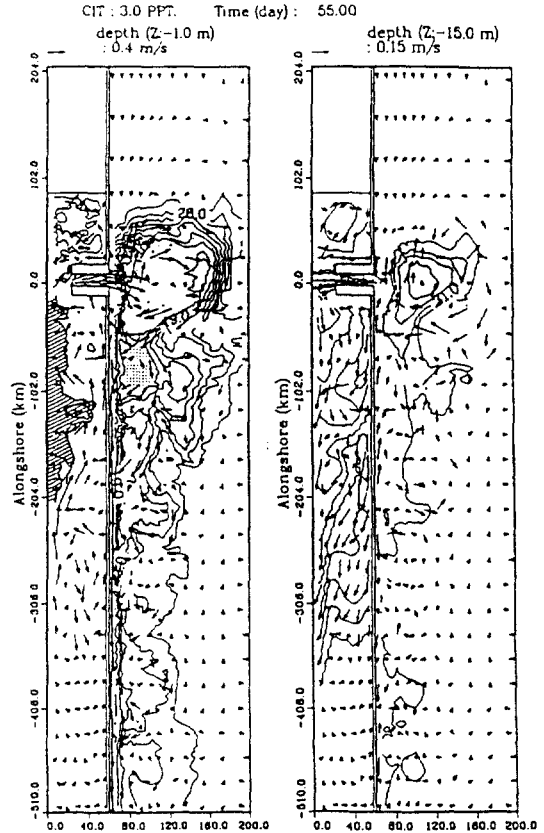
Fig. 5c. As in Fig. 5a except at time t=31 days.

Fig. 5d. As in Fig. 5a except at time t=55 days.

As in C1 case, the calculation in C2 also results in anticyclonic turn of the near-surface plume at the estuary mouth, and a coastal front which meanders alongshore. An energetic analysis for stability in this case also gives similar results: a short-time baroclinically unstable developing phase, and, eventually, a matured phase dominated by baroclinic instability for the final 60 days of the model integration. The last two phases are seen in Figs. 5a, 5b, and 5c as short-wave meanders along the coastal front for t=10 and 20 days change to longer waves for t>31 days.

There are also important differences between the two calculations. First, the flow in C2 is strongly baroclinic, and shows an almost two-layer vertical structure with energetic near-surface currents. The stratification-dependent eddy diffusivity in C2 limits vertical mixing of fresh and saline waters, and the estuarine water remains confined near the

surface as it discharges onto the shelf and along the coast. The outflow is highly inertial with maximum speeds reaching some 1.2 ms^{-1}. This is in contrast to the C1 case, which gives maximum outflow speeds of about 0.4 ms^{-1}. A consequence of the highly inertial and stratified nature of the flow field is that the bounding front of the plume is much stronger in C2 than that in C1. In Figs. 2a and 5a, the cross-frontal salinity difference is about 6.0‰ in C1, and is about 18.0‰ in C2, a three-fold increase in the frontal strength. The flow speed along the bounding front also increase. approximately in proportion to the frontal strength. An example of this increase is the offshore flow along the northern bounding front of the plume in Figs. 2a and 5a, a region into which outflow from the mouth of the estuary extends. The three-fold increase in the outflow speeds, quoted above, is therefore consistent with the three-
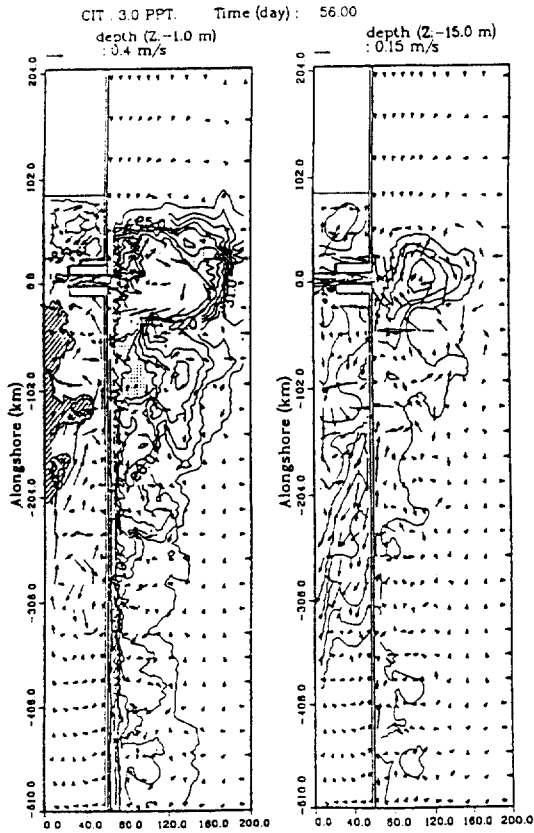
Fig. 5e. As in Fig. 5a except at time t=56 days.

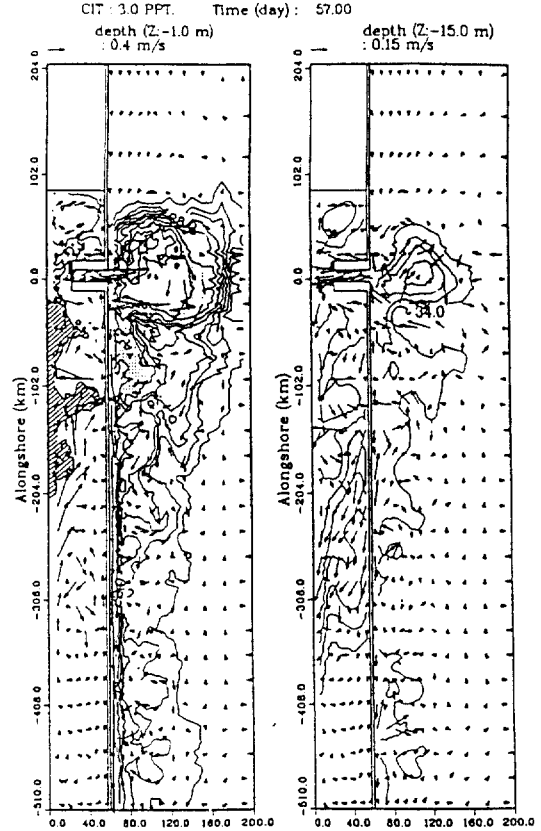
Fig. 5f. As in Fig. 5a except at time t=57 days.

fold increase in the frontal strength. Another example is the onshore flow along the northern bounding front of the plume. A comparison of Fig. 2 and Fig. 5 again shows an approximately three-fold increase in speeds (Figs. 2c and 5c, for example). The coastal frontal strength, hence the along-front velocity, are also correspondingly stronger for C2 than those for C1. This results in faster adjustment, for C2, of the coastal front set up passage of the initial southward intrusive bore. By 10 days, near-surface coastal front is developed with a strong along-coast jet.

Secondly, because of the stronger outflow in C2, supercritical flow state, for which the near-surface outflow velocity, u_0, exceeds the baroclinic phase speed C_i, can exist off the mouth of the estuary. According to Garvine (1984, 1987), frontal features develop off the mouth of an estuary when flow is supercritical. Thus the increased strengh of the

plume's bounding front in C2 can be interpreted as being the results of the supercritical outflow. Moreover, Garvine's (1984) result also shows development of internal hydraulic jump near the freshwater source and behind the bounding front of the plume. At some critical Froude number, $F_r = u_0$ /C_i, Garvine postulates that large mixing would occur at the jump, so that the near-surface, less-saline water downstream of the jump becomes detached from its source, to form eddy or ring. This process would repeat as bouyant water continuously discharges from the estuary. A rough estimate of C_i at the mouth of the estuary is

$$C_i = (gH \ d\rho/\rho_o)^{1/2}\pi = 0.8 \ ms^{-1} \tag{18}$$

where H is the water depth of 20.0 meters, and d is the top to bottom density difference, taken to be 28 kg/m^3 for the present model simulations. Therefore, the outflow is subcritical for C1, and
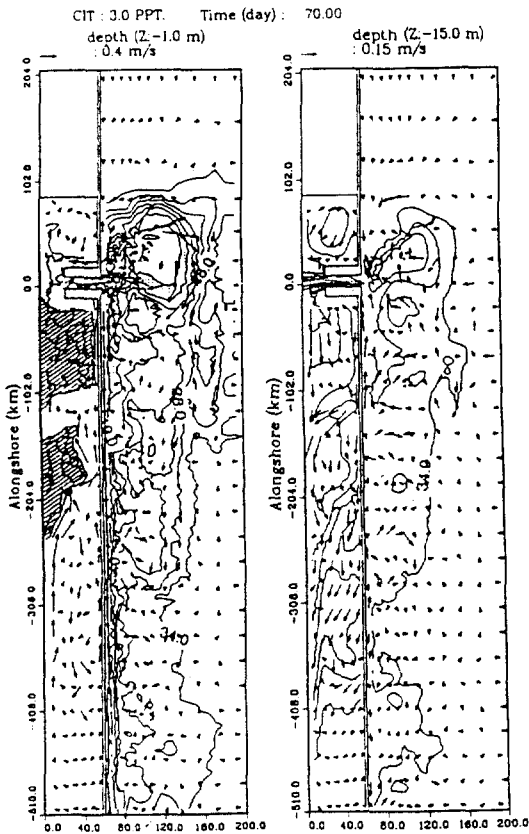
Fig. 5g. As in Fig. 5a except at time t=70 days.

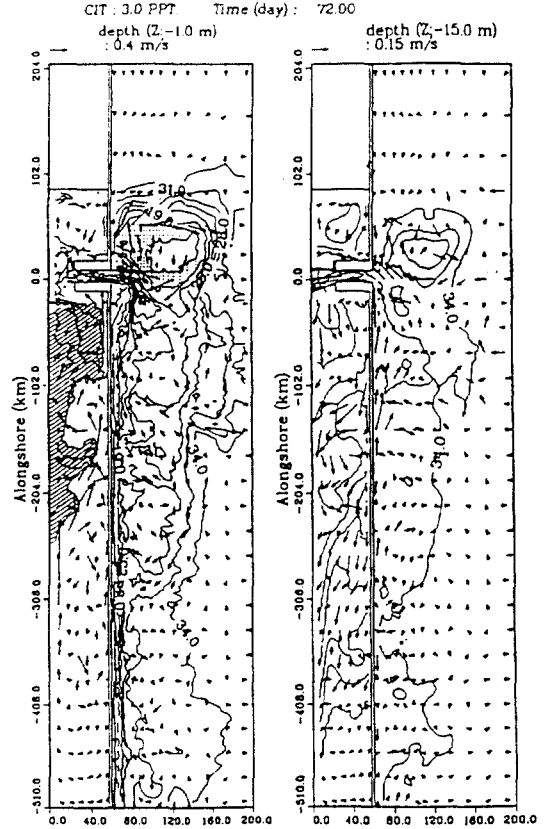
Fig. 5h. As in Fig. 5a except at time t=72 days.

near-critical/super-critical for C2. In C1, Figs. 2, the salinity contours show smooth variation from estuary's mouth onto the shelf, so that there is no evidence of formation of internal hydraulic jumps and/or ring-sheddings. In C2, Figs. 5, the salinity contours show large-scale (>10 km) patchness off the estuary's mouth and in the plume (Figs. 5b, c, d, f, h, and i). The occurrences of these detached rings fit fairly well the simpler descriptions obtained from Garvine's model.

Thirdly, the uni-directionality of the near-coast southward flows south of the main plume, as seen in Figs. 2 for C1, Figs. 5 for C2, often interrupted along the shoreline by episodic opposing flows near the bottom. (These events also exist for C1, but are much weaker.) The events are more clearly seen for t>31 days in Figs. 5. More detailed salinity and velocity plots reveal that the reversed flows are caused by southward progression of

shore-bound, less-salinity pools which leak out from the southern bounding front of the plume. An example of this leakage event is shown in Figs. 5b, e and f, in which the stippled regions south of the plume, where 16‰<S<19‰, are seen to advect southward. The progression of these pools of less-saline water and the frontal meander both give rise to intermittent coastal currents.

Finally, the adjustment process in the storage basin for C1 and C2 are quite different, dictated by the strongly baroclinic nature of the flow in C2. The storage basin can in the present case be thought of as a model for a wide, rectangular-shaped estuary or bay, and we examine what happens when there is a sudden intrusion of salt water through its northern opening; perhaps by upwelling-favorable wind over the adjacent shelf, say. In both C1 and C2, bottom intrusion occurs along the right-hand wall (for an observer at the nor-
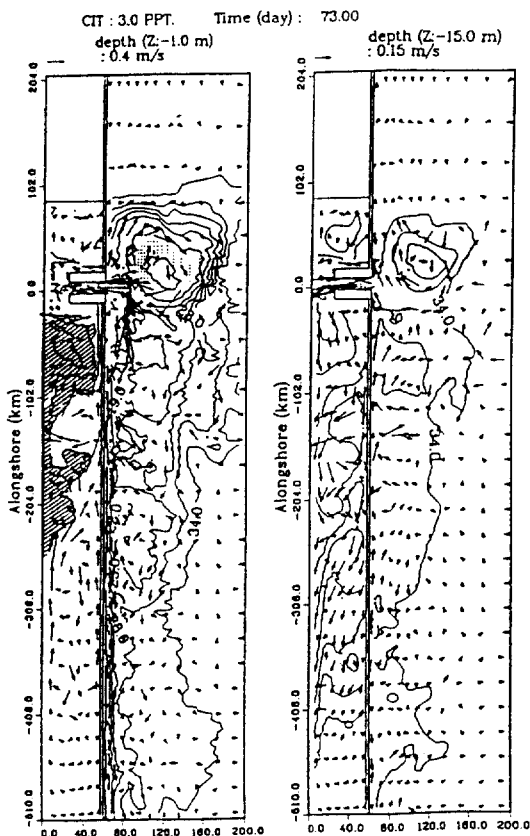
CIT : 3.0 PPT.   Time (day) :   73.00
depth (Z:-1.0 m)   depth (Z:-15.0 m)
: 0.4 m/s   : 0.15 m/s

Fig. 5i. As in Fig. 5a except at time t=73 days.

them opening looking southward up the bay). In C1, momentum of the bottom intrusion is uniformly mixed throughout the water column, with the results that the internal effects, as well as the vertical shear of the north/south component with the intrusion must, therfore, in part be balanced by an across-bay flow to the left, i.e. await from the right-hand wall. Thus salinity contours in Figs. 2 extend across the bay, and the right-bounded coastal current produced by the intrusion is weak and barely distinguishable. In C2, stratification prevents turbulence generated by the bottom intrusion to propagate into the upper layers. The inertial effects and vertical shears of the bottom intrusion to propagate into the upper layers. The inertial effects and vertical shears of the bottom intrusion are sufficient, therefore, to balance the north/south pressure gradient, and the right-bounded coastal current is intense. The response is clearly more

baroclinic than for C1, since one can easily discern bay-wise, cyclonic bottom and anticyclonic surface circulation upstream of the intrusive nose (Figs. 5a, b and c). The coastal current eventually develops instability and meander wave. One such example is shown in Figs. 5d through 5h, in which areas with salinity greater than 7.0‰ in the surface-layer are highlighted by cross hatches. Three distinct waves are seen in Figs. 5d through 5f. The wavelengh is approximately 60 km, or about $2\pi R_o$, which suggests instability of the baroclinic type. On the other hand, since forcing is from the bottom layers, the dynamics of intrusion is also relevant to the development of these waves. The development of near-surface meanders in the fresh water basin is a consequence of the flow adjustment in the bottom layers as potential energy fed by intrusion is converted into kinetic energy of the eddying motion. These eddies (and their associated meanders) are uni-directional (in the sense that surface and bottom layers acquire vorticity of the same sign) contrasts that found for the surface intrusion along the coast on the shelf, in which we noted less-saline water leaks southward of the main plume. This is because for the bottom intrusion, bottom friction is 2 or 3 times larger (due to the larger bottom velocity), resulting in more mixing, hence more coherent response in the vertical.

CONCLUSION

Two different turbulence parameterizations, one is the constant eddy-mixing formulaton (C1) and the other a stratification dependent eddy-mixing formulation (C2), are studied to examine the differential turbulence intensities in the water column.

The outflow onto ocean from an estuary is highly inertial and forms a strong front of plume in C2 than that in C1. Because of the stronger ouflow in C2, supercritical flow state can exist off the mouth of the estuary. The mixing adjustment process indictates the strongly baroclinic nature of the flow in C2. More active development of long waves characteristics of baroclinic instability process, in addition to shorter wave of barotropic

instability can be depicted in C2.

The time-dependent eddy-shedding occurred in the plume due primarily to formation of internal hydraulic jumps and intense mixing as flow exits the estuary onto the shelf. The plume itself eventually becomes unstable, which leads to intermittent coastal currents with time scales of the order of 5 to 12 days.

The present estuarine coastal model will serve as a basis for studies of estuary/shelf interaction problem, as well as for realistic simulation with real bathymetry and forcing for a particular coastal region of interest.

ACKNOWLEDGEMENTS

REFERENCES

Blumberg, A. F. and G. L. Mellor, 1983. Diagnostic and prognostic numerical circulation studies of the South Atlantic Bight. *J. Geophys. Res., Ocean*, **88**: 4579-4592.

Chao, S. -Y. and W. C. Boicourt, 1986. Onset of estuarine plumes. *J. Phys. Oceanogr.*, **16**: 2137-2149.

Chao, S. -Y., 1987. Wind-induced motion near inner shelf fronts. *J. Geophys. Res.*, **92**: 3849-3860.

Chao, S. -Y., 1988a. River-forced estuarine plumes. *J. Phys. oceanogr.*, **18**: 72-88.

Chao, S. -Y., 1988b. Wind-driven motion of estuarine plumes. *J. Phys. Oceanogr.*, **18**: 1144-1166.

Garvine, R. W., 1984. Radial spreading of bouyancy, surface plumes. *J. Geophys. Res.*, **89**: 1989-1996.

Garvine, R. W., 1987. Estuary plumes and fronts in shelf waters: a layer model. *J. Phys. Ocenogr.*, **17**: 1877-1896.

Mellor, G. L. and T. Yamada, 1982. Development of a turbulence closure model for geophysical fluid problems. *Rev. Geophys. Space Phys.*, **20**: 851-875.

Oey, L. -Y., G. L. Mellor and R. I. Hires, 1985. A three-dimensional simulation of the Hudson-Raritan stuary. Part I: Description of the model and model simulations. *J. Phys. Oceanogr.*, **15**: 1676-1692.

Oranski, I. and M. D. Cox, 1973. Baroclinic instability in ocean currents. *Geophyical Fluid Dynamics*, **4**: 297-332.

Oranski, I., 1976. A simple boundary condition for unbounded hyperbolic flows. *J. Comput. Phys.*, **21**: 251-269.

Stern, M. E., J. A. Whitehead and B. L. Hua, 1982. The intrusion of a density current along the coast of a rotating fluid. *J. Fluid Mach.*, **123**: 237-265.

You, K. W., L. Y. Oey, Y. H. Zhang, P. Chen, H. Jo, J. Manning, R. Patchen and J. Herring, 1991. A three-dimensional simulation of bouyancy and wind induced circulation and mixing in the New York Bight. *Estuarine and Coastal Modeling*, ASCE, 453-465.

You, K. W. and I. S. Oh, 1993. An effect of the eddy intrusive transport variations across the shelfbreak on the Korea Strait and the Yellow Sea. Part I: Barotropic model study. *J. Oceanol. Soc. Korea*, **28**: 281-291.